



ELSEVIER

Nuclear Physics A 645 (1999) 536–558

NUCLEAR
PHYSICS A

Shape evolution of the hot giant dipole resonance

Nguyen Dinh Dang^{a,b,1}, Kosai Tanabe^a, Akito Arima^{b,c}

^a Department of Physics, Saitama University, Urawa, Saitama 338-8570, Japan

^b RIKEN, Wako, Saitama 351-01, Japan

^c Ministry of Education, Chiyoda-ku, Tokyo, Japan

Received 26 August 1998; revised 29 October 1998; accepted 20 November 1998

Abstract

A systematic description of the evolution of the giant dipole resonance (GDR) at non-zero temperature T is given within the framework of two versions PDM-1 and PDM-2 of the Phonon Damping Model (PDM). The PDM interprets the damping of the GDR as a result of coupling to all ph , pp and hh configurations at $T \neq 0$, where the coupling to pp and hh configurations is decisively important for an adequate description of the increase and saturation of the GDR width as a function of T . The numerical calculations have been performed for the GDR width, the strength function and the integrated yield of the γ rays in ^{120}Sn and ^{208}Pb at $0 \leq T \leq 6$ MeV. The results obtained are found in a reasonable agreement with the most recent experimental data for all these three characteristics including the saturation of the yields within the GDR region and in the region above it. Predictions have been made for the GDR shape in both nuclei at T up to 6 MeV and for the integrated yield of γ rays in ^{208}Pb . © 1999 Elsevier Science B.V.

PACS: 21.10.Pc; 24.10.Pa; 24.30.Cz; 24.60.-k; 25.70.Gh

Keywords: Giant dipole resonance; Hot nuclei; Damping; Strength function

1. Introduction

The giant dipole resonance (GDR) built on compound states of highly excited nuclei (hot GDR) has been studied since the 1980s mostly using heavy-ion fusion reactions (see Ref. [1] for reviews). A broadening of the GDR width with increasing excitation energy E^* up to $E^* \sim 130$ MeV in tin isotopes has been observed [2–6]. At higher E^* a saturation of the GDR width has been reported [7,8]. Besides the width saturation the

¹ Visiting researcher of the Japan Society for the Promotion of Science. On leave of absence from the Institute of Nuclear Science and Technique – VAEC, Hanoi, Vietnam. E-mail: dang@rikaxp.riken.go.jp

heavy-ion fusion measurements also showed that the integrated yield of the γ -rays from the decay of the hot GDR in tin isotopes seemed to saturate at $E^* \geq 350$ MeV in the GDR region within $12 \text{ MeV} \leq E_\gamma \leq 20 \text{ MeV}$ [9,10] and in the region above 20 MeV ($20 \text{ MeV} \leq E_\gamma \leq 35 \text{ MeV}$) [10].

Considerable attention was paid to the effects of angular momentum J and temperature T on the evolution of the hot GDR. By gating on the γ -ray multiplicity in fusion-evaporation reactions one could select the angular momentum J and study its effects on the GDR at a given temperature T [4,5]. Existing data and calculations showed that the angular momentum effects seemed to be unimportant at least for spins $J \leq 36 \hbar$ and mass number $A \geq 120$ [5,7,11].

Recently a new method employing small-angle light-ion scattering to excite the nucleus has been proposed to study the evolution of the GDR as a function of temperature T independently of angular momentum effects [12,13]. Detailed systematics of the temperature dependence of both the width [12,13] and shape [13] of the GDR have been extracted with rather small errors in the temperature intervals $0 \leq T \leq 3.12$ MeV for ^{120}Sn and $0 \leq T \leq 2.05$ MeV for ^{208}Pb . In particular, Ref. [13] has shown that the GDR widths measured in inelastic α -scattering experiments and in fusion reactions do not differ much in their evolution with T while the angular momentum is about 10 to 20 \hbar lower in case of the inelastic scattering data. This is a clear indication that the effect of spin on the hot GDR in tin isotopes is not significant.

These experimental systematics opened new challenges facing the theoretical study of the hot GDR. In fact in the present situation an adequate approach to the damping of the hot GDR must give a consistent description of three following issues:

- (i) the width increase and its saturation of the GDR as a function of T ;
- (ii) the observed shape evolution of the GDR at various temperatures;
- (iii) the saturation of the integrated yield of γ rays at $E^* > 300$ MeV in the GDR region and in the region above it.

Among the most intensive theoretical studies devoted to the damping of the hot GDR in recent years we refer two models, which have been proposed by the Milan group [14,15] and Catania group [16–18], respectively. Their predictions have been frequently quoted by several experimental groups and compared with the data. The Milan model in Ref. [15] interprets the GDR broadening (issue (i)) via adiabatic coupling of the collective vibration to nuclear shape fluctuations. It describes well the width increase in both nuclei ^{120}Sn and ^{208}Pb at $T \leq 3$ MeV. The Catania model is based on the interplay between one-body Landau damping and two-body collisional damping of nucleons within the linearized Landau-Vlasov theory. It describes satisfactorily the width increase in ^{208}Pb but underestimates the width in ^{120}Sn by ~ 20 –30% within the same temperature region [13]. In the region $T > 3$ MeV where the observed width saturates these models give different trends for the GDR width. The Milan model in Ref. [14] interprets the width saturation as a consequence of the limitation of the maximum spin which a compound nucleus could reach. The Catania model gives a continuously increasing width, which becomes larger than 20 MeV at $T > 3$ –4 MeV. With such a large width the existence of the GDR itself is questionable. The result of

the Catania model is in favor of the disappearance of the GDR at high T . As a matter of fact, in order to fit their data on the saturation of the γ -ray yield in the GDR region in tin isotopes (issue (iii)) the authors of Ref. [9] have also introduced a width in the multistep CASCADE calculations, which increases sharply with increasing T . From this parametrization it has been concluded in Ref. [9] that the GDR gradually disappears at high temperature. However, recent measurements by the MEDEA collaboration [10] have shown that such a large width overestimates strongly the integrated yield of the γ rays in the region above the GDR ($20 \text{ MeV} \leq E_\gamma \leq 30 \text{ MeV}$) within the same multistep CASCADE calculations. The GDR cross-sections estimated using the width parametrizations by the Catania model and by Ref. [9] are also strongly enhanced in comparison with the data [6]. It has also been shown in Ref. [10] that the γ spectra in tin isotopes can be well described using a saturated value of 12 MeV for the GDR width and a cutoff of γ emission from the resonance above $E^* \sim 250 \text{ MeV}$. Meanwhile the authors of Ref. [19] have pointed out recently that not only the comparison of the calculated full width at half maximum (FWHM) with the experimental GDR width, but also the complete shape of the GDR strength function should be considered (issue (ii)) to achieve a meaningful comparison between theory and experiment. The detailed analysis in Ref. [19], which includes the entire shape of the strength function, has shown that neither the Milan model nor the Catania model can reproduce the observed GDR shape.

Recently we have proposed a microscopic model for the damping of the hot GDR [20], which will be referred to simply as the Phonon Damping Model (PDM) in short-hand hereafter. In the PDM the GDR is generated by a collective vibration (the GDR phonon), which is damped via coupling to all ph as well as pp and hh configurations appearing at $T \neq 0$. We have shown that the coupling to particle–particle (pp) and hole–hole (hh) configurations is decisively important for a consistent description of the width increase and its saturation. The application of the PDM in a systematic study of the hot GDR width in ^{90}Zr , ^{120}Sn , and ^{208}Pb has shown an overall agreement with the data [20] in a wide temperature interval $0 \leq T \leq 6 \text{ MeV}$, which covered both the regions of the width increase and its saturation. In view of the new revised data from the inelastic α -scattering experiments on the width and, in particular, the shape of the hot GDR [13], we would like to report in the present paper an application of the PDM and of its further elaboration to a systematic description for the width and shape of the hot GDR in ^{120}Sn and ^{208}Pb . The analysis is carried out with the aim to test the capability of our model in addressing three issues mentioned above. Finally we hope that the present study can shed a further light on the question under debate on whether the GDR disappears or still persists at high T .

The paper is organized as follows. In Section 2 the outline of the PDM is presented. In Section 3 the numerical results for the GDR width, its shape and the integrated yield of γ rays in ^{120}Sn and ^{208}Pb are presented and compared with the most recent experimental systematics in Ref. [13] and also Refs. [7–10]. Predictions for the shape of the GDR at higher temperatures up to $T \sim 6 \text{ MeV}$ are provided as references for measurements in future. The paper is summarized in the last section where conclusions are drawn.

2. Formalism

The PDM applies the double-time Green function method [21,22] to determine the physical processes which the GDR phonon undergoes and to derive a closed set of equations for the Green functions. The final goal is to obtain an approximate equation for the propagation of the GDR phonon, which is damped due to the presence of a polarization operator containing the effects of coupling to all ss' configurations ($(s, s') = (p, h), (p, p')$ and (h, h')). The damping of the GDR is defined as the imaginary part of the analytic continuation of the polarization operator into the complex energy plane.

In this section the outline of two approximation schemes of the PDM are presented in brief. The first one, which is referred to as PDM-1 hereafter, has been proposed and discussed in detail in Ref. [20]. The PDM-1 treats the effects of higher-order graphs such as $1s1s' \otimes$ phonon or/and two-phonon ones by selecting parameters of the model at $T = 0$. The second approximation scheme, which is referred to as PDM-2 hereafter, is a further development of our model to include explicitly all the forward-going processes up to two-phonon ones at $T \neq 0$ in the same order of the interaction strength.

Our formalism is based on a model Hamiltonian, which is composed of three terms, namely

$$H = \sum_s E_s a_s^\dagger a_s + \sum_q \omega_q Q_q^\dagger Q_q + \sum_{ss'q} F_{ss'}^{(q)} a_s^\dagger a_{s'} (Q_q^\dagger + Q_q). \tag{2.1}$$

The first term is the single-particle field, where a_s^\dagger and a_s are creation and destruction operators of a particle or hole state with energy $E_s = \epsilon_s - \epsilon_F$ with ϵ_s being the single-particle energy and ϵ_F the Fermi energy. The second term is the phonon field, where Q_q^\dagger and Q_q are the creation and destruction operators of a phonon with energy ω_q . The last term describes the coupling between the first two terms with $F_{ss'}^{(q)}$ denoting the coupling matrix elements. The indices s and s' denote particle ($p, E_p > 0$) or hole ($h, E_h < 0$), while the index q is reserved for the phonon state $q = \{\lambda, i\}$ with multipolarity λ (the projection μ of λ in the phonon index is omitted for simplicity). The sums over q run over $\lambda \geq 1$. For a more detailed discussion of this Hamiltonian we refer to our previous papers [20].

2.1. The PDM-1

The PDM-1 considers the following double-time Green functions, which describe in the standard notation [22]:

(1) The propagation of a free particle (or hole):

$$G_{s';s}(t - t') = \langle\langle a_{s'}(t); a_s^\dagger(t') \rangle\rangle, \tag{2.2}$$

2) The propagation of a free phonon:

$$G_{q';q}(t - t') = \langle\langle Q_{q'}(t); Q_q^\dagger(t') \rangle\rangle, \tag{2.3}$$

(3) The particle–phonon coupling in the single-particle field:

$$\Gamma_{s'q,s}^-(t-t') = \langle\langle a_{s'}(t) Q_q(t); a_s^\dagger(t') \rangle\rangle, \tag{2.4}$$

$$\Gamma_{s'q,s}^+(t-t') = \langle\langle a_{s'}(t) Q_q^\dagger(t); a_s^\dagger(t') \rangle\rangle, \tag{2.5}$$

(4) The transition between a nucleon pair and a phonon:

$$\mathcal{G}_{ss',q}^-(t-t') = \langle\langle a_s^\dagger(t) a_{s'}(t); Q_q^\dagger(t') \rangle\rangle. \tag{2.6}$$

A closed set of coupled equations for Green functions in Eqs. (2.2)–(2.6) has been obtained in Ref. [20], following the standard method of double-time Green functions [22] applied to the Hamiltonian in Eq. (2.1). After making the Fourier transform to the energy plane E and eliminating functions $\Gamma^-(E)$, $\Gamma^+(E)$ and $\mathcal{G}(E)$ by expressing them in terms of $G_{s,s'}(E)$ and $G_{q,q'}(E)$, a set of two equations has been obtained for $G_{s,s'}(E)$ and $G_{q,q'}(E)$, which describe the p (h) and phonon propagations, respectively. For the propagation of a single p (or h) state $s = s'$ and a single phonon state $q = q'$ these equations become

$$\begin{aligned} G_s(E) &= \frac{1}{2\pi} \frac{1}{E - E_s - M_s(E)}, \\ G_q^{(\text{PDM1})}(E) &= \frac{1}{2\pi} \frac{1}{E - \omega_q - P_q^{(\text{PDM1})}(E)}, \end{aligned} \tag{2.7}$$

where the mass operator $M_s(E)$ and the polarization operator $P_q^{(\text{PDM1})}(E)$ are

$$\begin{aligned} M_s(E) &= \sum_{q' s'} F_{ss'}^{(q')} F_{s' s}^{(q')} \left(\frac{\nu_{q'} + 1 - n_{s'}}{E - E_{s'} - \omega_{q'}} + \frac{n_{s'} + \nu_{q'}}{E - E_{s'} + \omega_{q'}} \right), \\ P_q^{(\text{PDM1})}(E) &= \sum_{ss'} F_{ss'}^{(q)} F_{s' s}^{(q)} \frac{n_s - n_{s'}}{E - E_{s'} + E_s}. \end{aligned} \tag{2.8}$$

The dampings $\gamma_s(\omega)$ of the single-particle state and $\gamma_q^{(\text{PDM1})}(\omega)$ of the phonon state are derived as the imaginary parts of the analytic continuation in the complex energy plane $E = \omega \pm i\epsilon$ of the mass $M_s(E)$ and polarization operators $P_q^{(\text{PDM1})}(E)$, respectively

$$\begin{aligned} \gamma_s(\omega) &= \pi \sum_{q' s'} F_{ss'}^{(q')} F_{s' s}^{(q')} [(\nu_{q'} + 1 - n_{s'})\delta(\omega - E_{s'} - \omega_{q'}) \\ &\quad + (n_{s'} + \nu_{q'})\delta(\omega - E_{s'} + \omega_{q'})], \end{aligned} \tag{2.9}$$

$$\gamma_q^{(\text{PDM1})}(\omega) = \pi \sum_{ss'} F_{ss'}^{(q)} F_{s' s}^{(q)} (n_s - n_{s'})\delta(\omega - E_{s'} + E_s). \tag{2.10}$$

The single-particle occupation number n_s (for phonon ν_q) in Eqs. (2.8)–(2.10) has the form of a Fermi (Bose) distribution folded with a distribution of Breit–Wigner type with an ω -dependent width $2\gamma_s(\omega)$ ($2\gamma_q(\omega)$) and centered at $\tilde{E}_s = E_s + M_s(\tilde{E}_s)$ ($\tilde{\omega}_q = \omega_q + P_q^{(\text{PDM1})}(\tilde{\omega}_q)$). If γ_s is small, n_s can be well approximated by an exact Fermi distribution function with energy \tilde{E}_s . For ν_q this is not valid because γ_q can be large.

The main approximation of the PDM-1 consists of closing the hierarchy of the Green functions to Eqs. (2.2)–(2.6) based on the following decoupling approximation, which is originated from the approximate second quantization [21] and modified thermodynamically for the non-zero temperature case:

$$\langle\langle a_{s_1} \underbrace{Q_q^\dagger Q_{q'}}_{}; a_s^\dagger \rangle\rangle = \delta_{qq'} \nu_q G_{s_1;s}, \quad \langle\langle a_{s_1} \underbrace{Q_{q'} Q_q^\dagger}_{}; a_s^\dagger \rangle\rangle = \delta_{qq'} (1 + \nu_q) G_{s_1;s}, \tag{2.11}$$

$$\langle\langle \underbrace{a_{s_1}^\dagger a_{s_1}}_{} (Q_{q'}^\dagger + Q_{q'}) ; Q_q^\dagger \rangle\rangle = \delta_{ss'} n_s G_{q';q}, \quad \langle\langle \underbrace{a_{s_1}^\dagger a_{s_1}}_{} a_{s_1} ; a_s^\dagger \rangle\rangle = \delta_{s's_1} (1 - n_{s'}) G_{s'_1;s}. \tag{2.12}$$

This restricts the couplings in the mass operator $M_s(E)$ to at most $2p1h$ configurations if the phonon operator generates the collective ph excitation. The contribution of coupling to higher-order Green functions of “ $1p1h \oplus$ phonon” or two-phonon type which causes the quantal (spreading) width Γ_Q of the ground-state (g.s.) GDR is assumed to be independent of T and included effectively by selecting the parameters of the model at $T = 0$. The justification of this approximation comes from the fact that the quantal width Γ_Q depends weakly on T as has been shown by several numerical calculations in Refs. [23–25] and will be confirmed in the PDM-2 version of our model below.

2.2. The PDM-2

The PDM-2 includes explicitly the coupling to all forward-going processes up to two-phonon ones by introducing in addition to the Green functions in Eqs. (2.2)–(2.6) the following double-time Green functions which describe:

(5) The transition between a $1p1h \otimes$ phonon ($1p1p \otimes$ phonon or $1h1h \otimes$ phonon) configuration and a phonon:

$$F_{ss'q';q}^{-,+}(t - t') = \langle\langle a_s^\dagger(t) a_{s'}(t) Q_{q'}(t); Q_q^\dagger(t') \rangle\rangle, \tag{2.13}$$

(6) The transition between two- and one-phonon configurations:

$$G_{q_1q_2}^{-,+}(t - t') = \langle\langle Q_{q_1}(t) Q_{q_2}(t); Q_q^\dagger(t') \rangle\rangle. \tag{2.14}$$

The backward-going processes described by the Green functions

$$G_{q';q}^{+,+}(t - t') = \langle\langle Q_{q'}^\dagger(t); Q_q^\dagger(t') \rangle\rangle, \\ F_{ss'q';q}^{+,+}(t - t') = \langle\langle a_s^\dagger(t) a_{s'}^\dagger(t) Q_{q'}^\dagger(t); Q_q^\dagger(t') \rangle\rangle, \\ G_{q_1q_2;q}^{+,+}(t - t') = \langle\langle Q_{q_1}^\dagger(t) Q_{q_2}^\dagger(t); Q_q^\dagger(t') \rangle\rangle$$

are neglected because the poles of their Fourier transforms would be located at negative energies faraway from the GDR region. Hence, just like the Y -amplitudes in the random-phase approximation (RPA), they are not expected to affect noticeably the damping of GDR.

A set of coupled equations for an hierarchy of Green functions has been derived applying again the standard procedure described in Ref. [22]. Employing the decoupling scheme similar to Eqs. (2.11) and (2.12) we closed this set to the functions (2.2)–(2.6), (2.13) and (2.14). Making then the Fourier transform to the energy plane E and performing several simple manipulations to express the Fourier transforms of other functions in the set in terms of the Fourier transform of function (2.3) by using the same decoupling scheme, we end up with the final expression for the propagation of a single phonon ($q = q'$) as

$$G_q^{(\text{PDM2})}(E) = \frac{1}{2\pi} \frac{1}{E - \omega_q - P_q^{(\text{PDM2})}(E)}. \quad (2.15)$$

The explicit for of the polarization operator $P_q^{(\text{PDM2})}(E)$ in Eq. (2.15) is

$$P_q^{(\text{PDM2})}(E) = \sum_{s,s',s_1,q'} \frac{F_{ss'}^{(q)}}{E - E_{s'} + E_s} \times \left[\frac{F_{s's_1}^{(q')} \mathcal{M}_{ss_1}^{qq'}(E)}{E - E_{s_1} + E_s - \omega_{q'}} - \frac{F_{s_1s}^{(q')} \mathcal{M}_{s_1s'}^{qq'}(E)}{E - E_{s'} + E_{s_1} - \omega_{q'}} \right], \quad (2.16)$$

where the vertex function $\mathcal{M}_{ss'}$ is

$$\begin{aligned} \mathcal{M}_{ss'}^{qq'}(E) = & \sum_{s_2} \left\{ \frac{(1 - n_{s'} + \nu_{q'}) (n_s - n_{s_2})}{E - E_{s_2} + E_s} F_{s's_2}^{(q')} F_{s_2s}^{(q)} \right. \\ & - \frac{(n_s + \nu_{q'}) (n_{s_2} - n_{s'})}{E - E_{s'} + E_{s_2}} F_{s_2s}^{(q')} F_{s's_2}^{(q)} \\ & \left. + n_{s_2} (n_s - n_{s'}) \left[\frac{F_{s's}^{(q)} F_{s_2s_2}^{(q')}}{E - \omega_q - \omega_{q'}} + \delta_{qq'} \sum_{q_1} \frac{F_{s's}^{(q_1)} F_{s_2s_2}^{(q_1)}}{E - \omega_{q_1} - \omega_{q'}} \right] \right\}. \quad (2.17) \end{aligned}$$

The phonon damping $\gamma_q^{(\text{PDM2})}(\omega)$ is again defined as the analytic continuation of the polarization operator $P_q^{(\text{PDM2})}(E)$ in Eq. (2.16) into the complex energy plane, namely

$$\gamma_q^{(\text{PDM2})}(\omega) = |\text{Im} P_q^{(\text{PDM2})}(\omega \pm i\epsilon)|. \quad (2.18)$$

The function $P_q^{(\text{PDM2})}(E)$ in Eq. (2.16) includes all $1s1s'$, $1s1s' \otimes$ phonon ($(s, s') = (p, h), (p, p')$ and (h, h')) and two-phonon processes at the same second order in $F_{ss'}^{(q)}$. In the limit of high temperature the vertex function $\mathcal{M}_{ss'}^{qq'}(E)$ in Eqs. (2.16) and (2.17) tends to

$$\begin{aligned} \mathcal{M}_{ss'}^{qq'}(E)|_{T \rightarrow \infty} \rightarrow & \frac{1}{4} \sum_{s_2} \left\{ \frac{1}{\omega_{q'}} \left[\frac{E_{s_2} - E_s}{E - E_{s_2} + E_s} F_{s's_2}^{(q')} F_{s_2s}^{(q)} + \frac{E_{s_2} - E_{s'}}{E - E_{s'} + E_{s_2}} F_{s_2s'}^{(q')} F_{s's_2}^{(q)} \right] \right. \\ & \left. + \frac{1}{2T} (E_{s'} - E_s) \left[\frac{F_{s's}^{(q)} F_{s_2s_2}^{(q')}}{E - \omega_q - \omega_{q'}} + \delta_{qq'} \sum_{q_1} \frac{F_{s's}^{(q_1)} F_{s_2s_2}^{(q_1)}}{E - \omega_{q_1} - \omega_{q'}} \right] \right\}, \quad (2.19) \end{aligned}$$

which means that it decreases as $O(T^{-1})$ with increasing T because of the factor T^{-1} in front of two-phonon terms on the r.h.s. of Eq. (2.19). Neglecting these two-phonon processes would lead to a constant width at high temperature because the first two terms on the r.h.s. of Eq. (2.19) are independent of T provided $F_{ss'}^{(q)}$, E_s and ω_q do not or depend weakly on T . More details on the derivation of the PDM-2 equations and their diagrammatic illustration in connection with the NFT [23] are given elsewhere [26].

2.3. GDR parameters and integrated yield of γ rays

The GDR energy ω_{GDR} is determined within the PDM at the pole $\bar{\omega}$ of $G_q^{(i)}(\omega)$, i.e.

$$\bar{\omega} - \omega_q - P_q^{(i)}(\bar{\omega}) = 0, \tag{2.20}$$

where $\bar{\omega}$ is real and $P_q^{(i)}(\bar{\omega})$ is the real part of $P_q^{(i)}(E)$ with $P_q^{(i)}(E)$ being defined from Eq. (2.8) ($i = \text{PDM1}$) or Eq. (2.16) ($i = \text{PDM2}$).

The FWHM Γ_{GDR} of the GDR at energy ω_{GDR} is defined as twice as much as the phonon damping $\gamma_q^{(i)}(\omega)$

$$\Gamma_{\text{GDR}}^{(i)} = 2\gamma_q^{(i)}(\omega = \bar{\omega}). \tag{2.21}$$

The shape of the GDR is described by the strength function $S_q^{(i)}(\omega)$, which is derived from the spectral intensity $J_q^{(i)}(\omega)$ in the standard way using the analytic continuation of the Green function $G_q^{(i)}(\omega \pm i\epsilon)$ [21] and by expanding $P_q^{(i)}(\omega)$ around $\bar{\omega}$ [22]. The final form of $S_q^{(i)}(\omega)$ is

$$S_q^{(i)}(\omega) = \frac{1}{\pi} \frac{\gamma_q^{(i)}(\omega)}{(\omega - \bar{\omega})^2 + [\gamma_q^{(i)}(\omega)]^2}. \tag{2.22}$$

Since the damping $\gamma_q^{(i)}(\omega)$ depends on the energy variable ω , which runs over the γ -ray energy E_γ , the shape of the strength function $S_q^{(i)}(\omega)$, strictly speaking, is not given by a single Breit–Wigner curve. The spectral intensity $J_q^{(i)}(\omega)$ is related to the strength function $S_q^{(i)}(\omega)$ as

$$J_q^{(i)}(\omega) = \frac{S_q^{(i)}(\omega)}{e^{\omega/T} - 1}. \tag{2.23}$$

This form is proportional to the exponential shape of the γ -ray spectra observed in experiments while the strength function $S_q^{(i)}(\omega)$ can be directly compared with the divided spectra in the linear scale normalized by a strength constant.

The value of the FWHM of the GDR $\Gamma_{\text{GDR}}^{(i)}$ given by Eq. (2.21) is more reliable than the width extracted from the energy dispersion

$$\sigma = \sqrt{(\overline{E^2}) - (\overline{E})^2}, \quad \overline{E^k} = \frac{\int_{E_1}^{E_2} \omega^k S_q(\omega) d\omega}{\int_{E_1}^{E_2} S_q(\omega) d\omega} \quad (k = 1, 2), \tag{2.24}$$

because the variance σ is sensitive to the choice of cutoff energies E_1 and E_2 introduced in the distant wings of the strength distribution, especially when the strength function

is described by a Lorentzian or a Breit–Wigner curve. Meanwhile the empirical widths are the FWHM, which can be described by Γ_{GDR} in Eq. (2.21).

The present formalism considers the hot GDR, its width and shape as a result of averaging over the grand canonical ensemble at a given temperature. This temperature of a one-step statistical process may be compatible with the effective temperature that one would obtain by averaging over the multistep process in the CASCADE calculations. Therefore the yield of the γ -ray can be calculated here following the standard statistical model using simplifying assumptions. They include a T^2 -dependence for the neutron-decay width and the first-order of the logarithmic expansion of the level density [27]. This allows us to calculate the integrated yield $Y_\gamma^{(i)}$ within the interval $E_1 \leq \omega \leq E_2$ as follows:

$$Y_\gamma^{(i)} \propto \frac{1}{T^2} \int_{E_1}^{E_2} \omega^3 J_q^{(i)}(\omega) e^{(B_n/T)} d\omega, \quad (2.25)$$

where B_n represents the neutron binding energy and $J_q(\omega)$ is the spectral intensity defined in Eq. (2.23). This quantity should be compared with the empirically extracted yield, where a Lorentzian strength function $f_{\text{GDR}}(\omega)$ multiplied by $\exp(-\omega/T)$ was used instead of $J_q^{(i)}(\omega)$ [1]. We have checked that in the region of the GDR peak a Lorentzian distribution centered at ω_{GDR} with a FWHM Γ_{GDR} has almost the same shape as the Breit–Wigner one divided by ω_{GDR} with the same width.

3. Numerical results

3.1. Ingredients of numerical calculations

The PDM assumes that the GDR is generated by a single collective and structureless phonon with energy ω_q close to the energy ω_{GDR} . The single-particle energies defined in the Woods–Saxon potentials at $T = 0$ were used in calculations. The levels near the Fermi surface for ^{208}Pb are replaced with the empirical ones. The procedure of selecting ω_q and the matrix elements $F_{ss'}^{(q)}$ of the coupling to ph , pp and hh configurations is as follows.

In the PDM-1 the coupling matrix elements $F_{ss'}^{(q)}$ are parametrized as $F_{ph}^{(q)} = F_1$ for $(s, s') = (p, h)$ and $F_{pp'}^{(q)} = F_{hh'}^{(q)} = F_2$ for $(s, s') = (p, p')$ or (h, h') . As the ph interaction in the GDR is dominated only across two major shells, that are closest to the both sides of the Fermi surface, the uniform distribution of the ph matrix elements over all the levels can be justified if $F_1^2 \ll F_2^2$, as has been mentioned in Ref. [20]. Within a fully microscopic approach, where the phonon structure can be determined from the RPA, the PDM parameters can be expressed in terms of the X, Y amplitudes, and the matrix elements of the effective two-body interaction. However, this is beyond the scope of the present approach. In general, the PDM-2 contains the explicit coupling to phonons with different multipolarities λ . The calculations in Ref. [15] have shown

Table 1
PDM-2 parameters.

	ω_q (MeV)	$F_1^{(1)}$ (MeV)	$F_2^{(1)}$ (MeV)	r
^{120}Sn	17.0	6.261×10^{-3}	1.845×10^{-1}	8.603×10^{-2}
^{208}Pb	13.8	2.7×10^{-3}	9.95×10^{-2}	8.8×10^{-1}

that the major contribution of the shape fluctuations in the increase of the GDR width at $T \neq 0$ comes from the quadrupole shape fluctuations. In the present application of the PDM-2, as a test for the effect of coupling to quadrupole vibration we retain only dipole and quadrupole phonons in the two-phonon configuration mixing. Consequently, from the sums on the r.h.s. of Eqs. (2.16) and (2.17) there remain only one dipole phonon with $q = q'$, which corresponds to the GDR ($\lambda = 1$) and one quadrupole phonon with q_1 with energy close to the energy $E_{2_1^+}$ of the first quadrupole state ($\lambda = 2$). The values of ω_q and F_1 (within PDM-1) or $F_1^{(1)}$ (within PDM-2) have been selected so that the solution $\bar{\omega}$ of Eq. (2.20) is equal to the empirical value of ω_{GDR} while $\Gamma_{\text{GDR}}(\bar{\omega})$ reproduces the empirical FWHM of the g.s. GDR (i.e. the quantal width Γ_Q at $T = 0$). The value of F_2 (for PDM-1) or $F_2^{(1)}$ (for PDM-2) has been chosen so that the energy $\bar{\omega}$ is stable against varying T . In PDM-2 we first set the ratio $r = F_i^{(2)}/F_i^{(1)}$ ($i = 1, 2$) when choosing ω_q , $F_1^{(1)}$ and $F_1^{(2)}$ in order to achieve a stable solution for Eq. (2.20). These parameters are kept unchanged when T is varied. This ensures that all the T -dependence comes from dynamical effects of configuration mixing, and not due to adjusting parameters. The smearing parameter ε in Eq. (2.18) was chosen to be 0.5 MeV. The results were found to be stable against varying ε within $0.2 \text{ MeV} \leq \varepsilon \leq 1.0 \text{ MeV}$. The dipole sum rule was also checked to be conserved against varying T . The PDM-1 parameters ω_q , F_1 and F_2 (three parameters) have been given in Ref. [20]. The selected values of the PDM-2 parameters ω_q , $F_1^{(1)}$, $F_2^{(1)}$ and r (four parameters) for ^{120}Sn and ^{208}Pb are presented in Table 1. The values of the PDM-2 parameters differ noticeably from those in PDM-1 because the effects of higher-order graphs are explicitly included in the equations of the PDM-2.

3.2. Temperature dependence of GDR width

The GDR widths Γ_{GDR} calculated within two versions of the PDM are shown in Fig. 1a for ^{120}Sn and in Fig. 1b for ^{208}Pb . They are compared with the revised data from inelastic α -scattering experiments [13] and also from Refs. [7,8]. The values of the width obtained within the PDM-1 (dotted and dashed curves) have been reported previously Ref. [20]. It is seen that the theoretical curves in both versions of the PDM reproduce reasonably well the data including the width saturation at $T \geq 3$ –4 MeV in case of ^{120}Sn [7,8]. The values of the width obtained within the PDM-2 (solid and dash-dotted curves) are somewhat smaller than those calculated in PDM-1 at $T \geq 1.5$ –2 MeV in ^{120}Sn and $T \geq 0.7$ –0.8 MeV in ^{208}Pb . The reason is that in the PDM-1 the

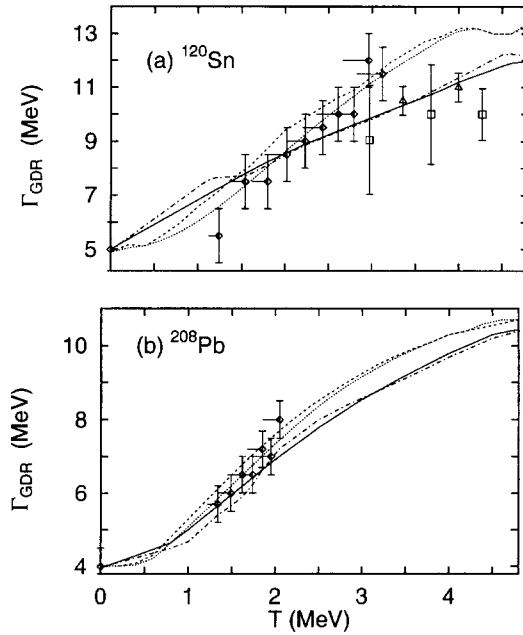


Fig. 1. Total width of GDR as a function of T for (a) ^{120}Sn and (b) ^{208}Pb . Dotted: results within PDM-1 without the effect of single-particle damping. Dashed: results within PDM-2 including the effect of single-particle damping. Solid: results within PDM-2 without the effect of single-particle damping. Dash-dotted: results within PDM-2 including the effect of single-particle damping. Squares, triangles and diamonds: data from Refs. [7], [8] and [13], respectively.

coupling to all multiplicities is included effectively in a sense of average, while in the PDM-2 the present calculation includes only one dipole phonon and one quadrupole phonon in the doorways. On the other hand the slight difference between the results obtained in two approximations indicates the importance of mixings with $\lambda = 1$ and 2 in reproducing the hot GDR width and shape as will be seen later. The effect of the single-particle damping on the GDR width is seen to be weak in both versions of the PDM by comparing the solid curve obtained without this effect with the dash-dotted curve calculated with taking into account this effect in PDM-2. Similarly, one should compare the dotted and dashed curves for PDM-1.

It has been shown in PDM-1 [20] that the total width is composed of the quantal width Γ_Q due to coupling of the GDR phonon to ph configurations and the thermal width Γ_T due to coupling to pp and hh configurations at $T \neq 0$. One of the main conclusions of Ref. [20] was that the behavior of the total width at high temperatures is mostly driven by the thermal width Γ_T since the quantal width Γ_Q decreases slightly as temperature increases. In order to see whether this conclusion still holds within the PDM-2 which includes higher-order processes up to two-phonon ones, we have performed the calculations of Γ_Q by switching off the coupling to pp and hh configurations in the sums on the r.h.s. of Eqs. (2.16) and (2.17). The results are displayed in Fig. 2 by solid curves which show a clear decrease as T increases. Exclusion of two-phonon terms

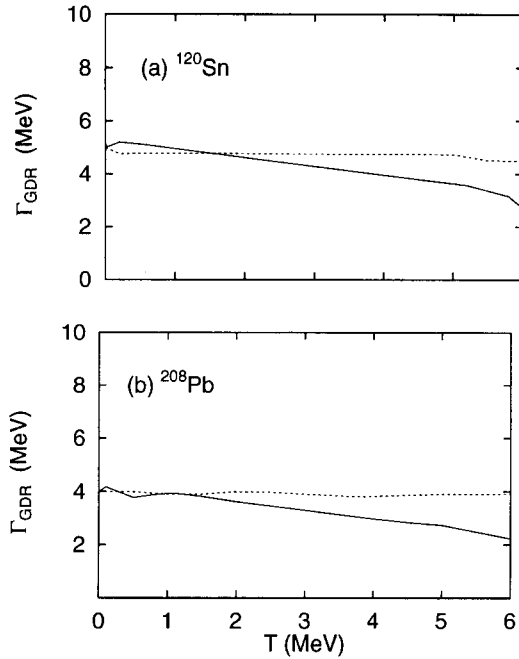


Fig. 2. Quantal width Γ_Q as a function of T for (a) ^{120}Sn and (b) ^{208}Pb . Solid: quantal width Γ_Q obtained within PDM-2. Dashed: quantal width Γ_Q obtained within PDM-2 when the contribution of the two-phonon processes at $T \neq 0$ is omitted.

at $T \neq 0$ in Eq. (2.17) results in a quantal width, which is practically independent of T (dashed curves) in agreement with the conclusion of Refs. [23,25].

3.3. Evolution of GDR shape

The GDR strength function $S_q^{PDM1}(\omega)$ calculated within the PDM-1 is compared with the normalized experimental one $f_{E1}(E_\gamma)$ [13] in Fig. 3 for ^{120}Sn and Fig. 4 for ^{208}Pb .

The experimental values of E_γ have been shifted up by 1.5 MeV in ^{120}Sn and by 1 MeV in ^{208}Pb in order to achieve a best agreement. This is due to the fact that the PDM assumes a temperature-independent GDR energy ω_{GDR} equal to the energy of the g.s. GDR. The solution $\bar{\omega}$ of Eq. (2.20) has been found to be stable around 15.4 MeV for ^{120}Sn and 13.5 MeV for ^{208}Pb at all temperatures using the selected values of the parameters in both versions PDM-1 and PDM-2. Meanwhile the experimental resonance energy was found in Ref. [13] to be lower than the g.s. GDR energy by an amount roughly equal to this shift. In other measurements the g.s. GDR energy ($T = 0$) has been used for the best fit of the data at $T \neq 0$ [2,4–9]. At present no systematic dependence of the GDR energy on the excitation energy E^* (or temperature T) has been confirmed and more studies are called for to resolve this issue. Therefore we do not consider reasonable at this stage to vary the parameters of our model with temperature to achieve the decrease of the GDR energy in Ref. [13]. Inclusion of this energy shift yields

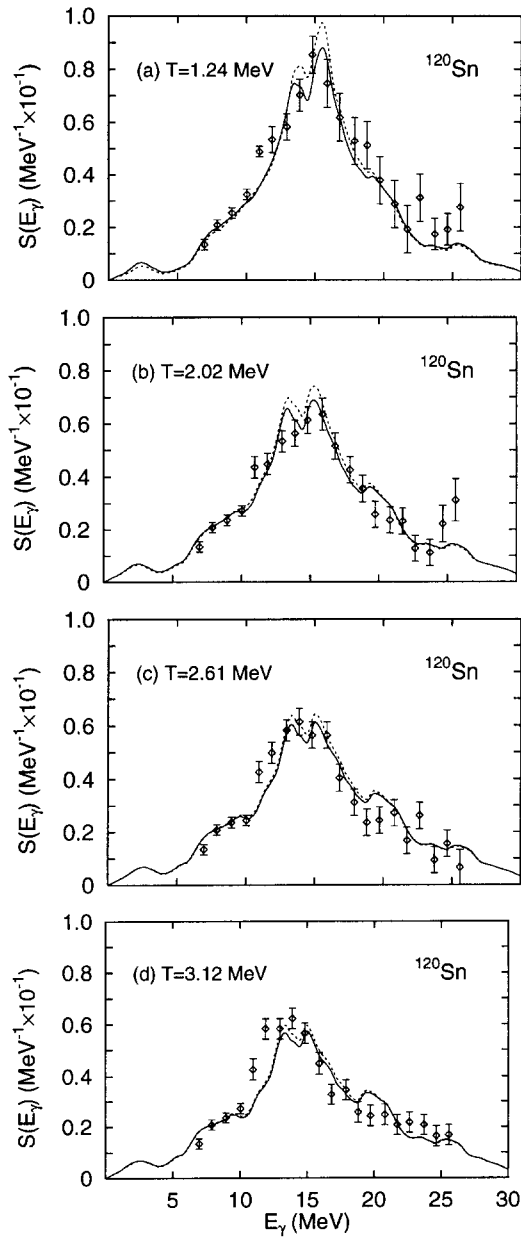


Fig. 3. GDR strength function in ^{120}Sn calculated within PDM-1 at several temperatures. Solid: results obtained with the effect of single-particle damping. Dashed: results without the effect of single-particle damping. Diamonds: normalized data from Ref. [13].

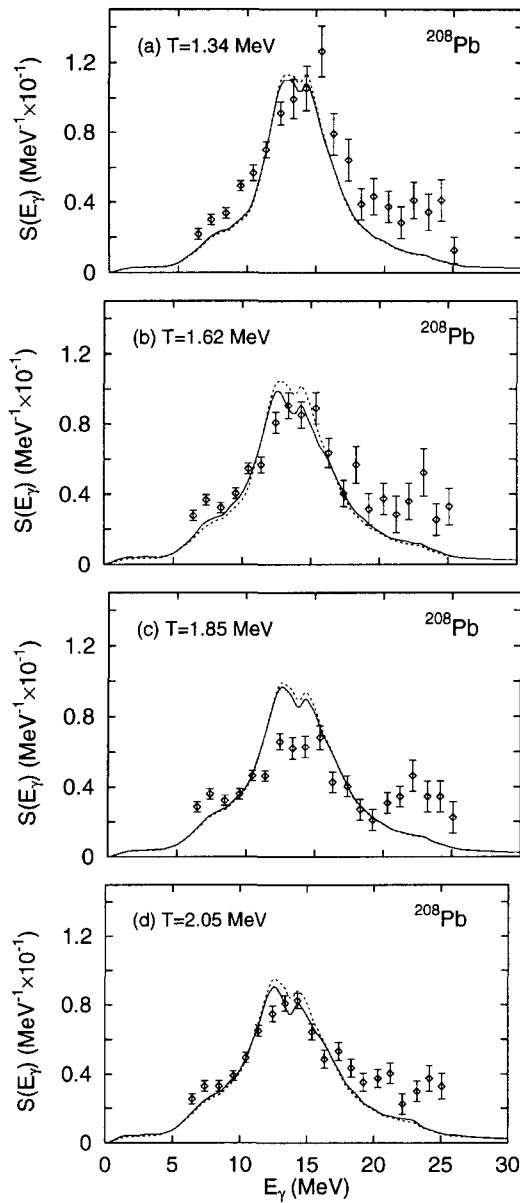


Fig. 4. Same as Fig. 3 for ^{208}Pb .

a good agreement between the calculations in PDM-1 and the available data for the evolution of the GDR shape in ^{120}Sn (Fig. 3). The PDM-1 could even reproduce the fine structure on two shoulders of the experimental resonance peak, especially the one in the low-energy region. For ^{208}Pb the data do not strictly follow a Breit-Wigner or Lorentzian shape. At $T = 1.85$ MeV the experimental shape of the GDR has even a pronounced structure between 20–25 MeV while the resonance peak seems to be too

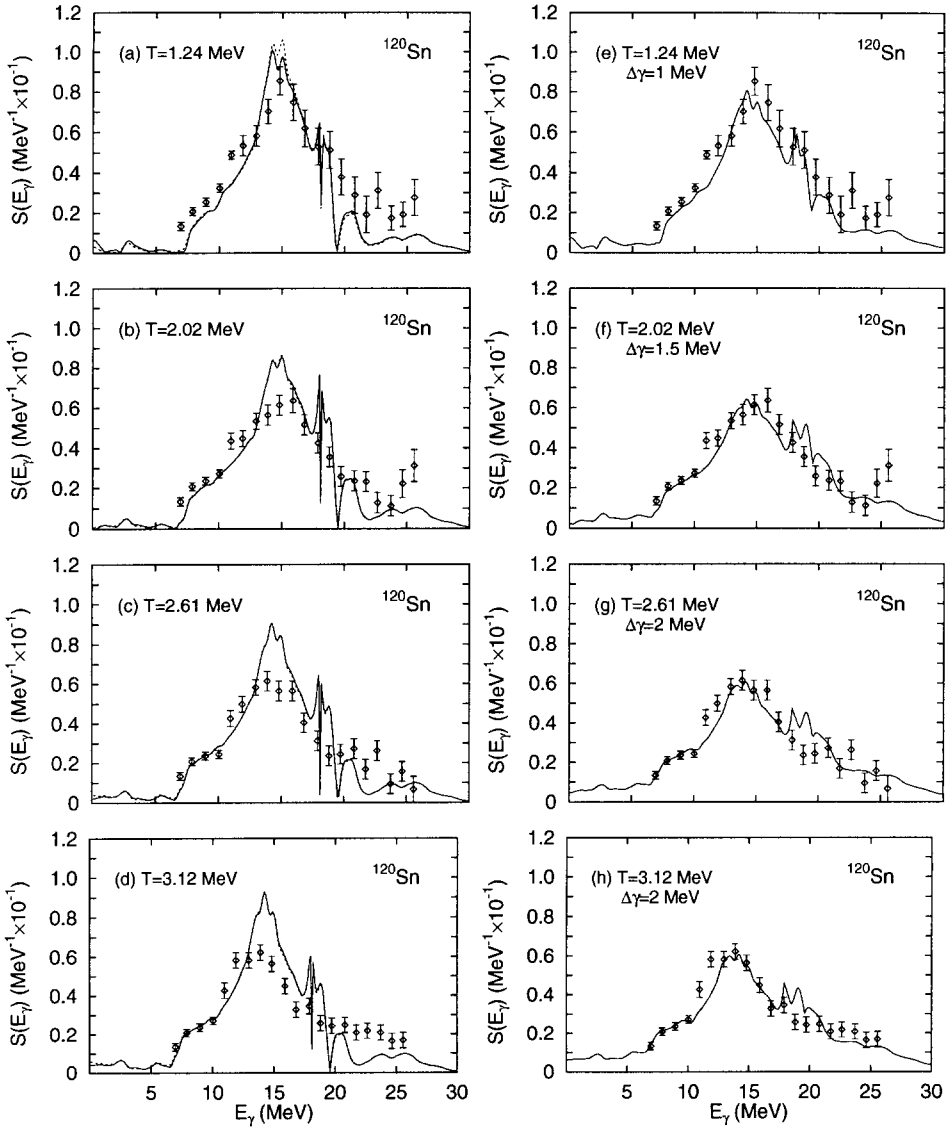


Fig. 5. GDR strength function in ^{120}Sn calculated within PDM-2 at several temperatures. Notation is the same as in Fig. 3. (e–h): Results of calculations using $\gamma_q^{(\text{PDM2})}(\omega) + \Delta\gamma$ instead of $\gamma_q^{(\text{PDM2})}(\omega)$ are shown with the corresponding values of $\Delta\gamma$.

low. Nonetheless the agreement between the results of calculations in the PDM-1 and the data for ^{208}Pb is also satisfactory (Fig. 4).

Shown in the left columns (a–d) of Figs. 5 and 6 are the results of calculations within PDM-2 and the same data from Figs. 3 and 4. Since the present version of the PDM-2 restricts the coupling to ph , pp and hh configurations via the doorways, which included only dipole and quadrupole phonons, the calculated shape is found slightly narrower and higher at its peak position. This restriction also causes some structure between 15 and

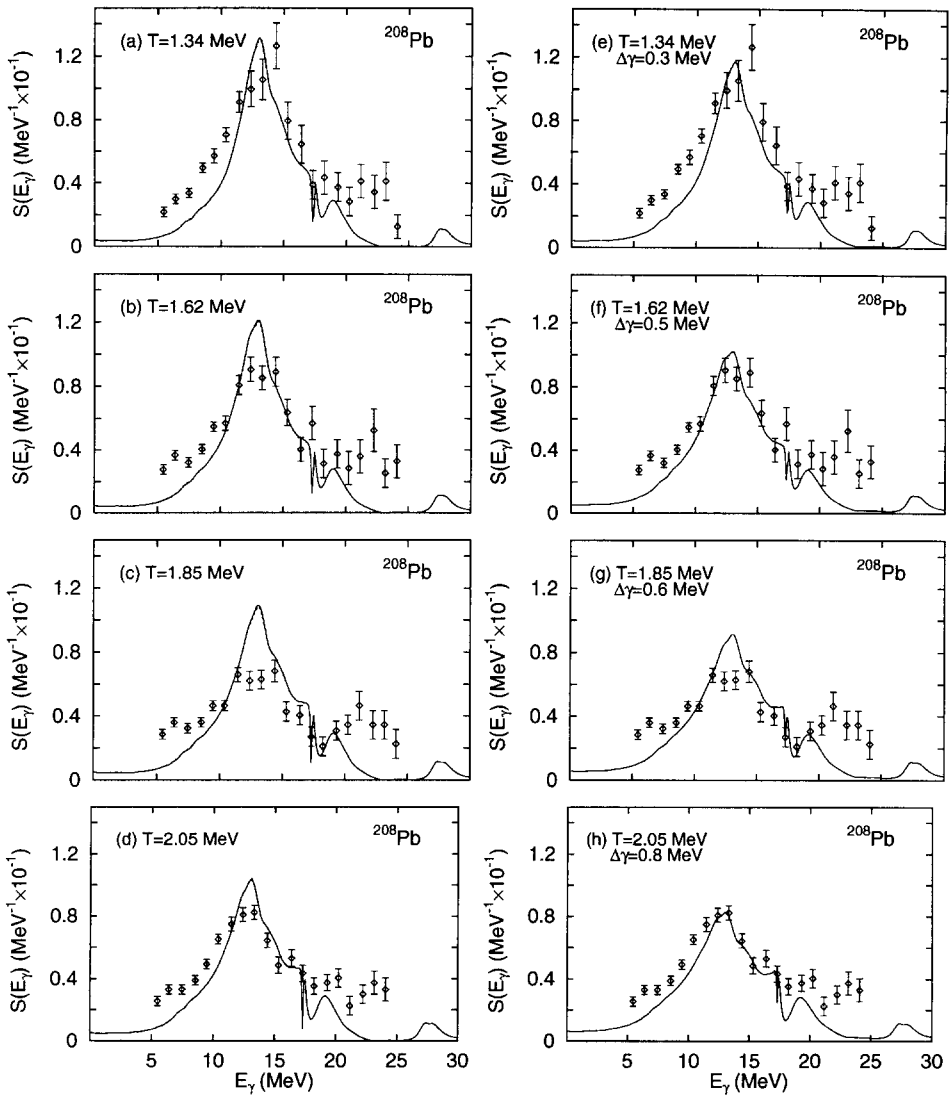


Fig. 6. Same as Fig. 5 for ^{208}Pb .

20 MeV at energies around $\omega_q + \omega_{q_1}$. Nonetheless an overall agreement between theory and data is achieved also in PDM-2. Taking into account more collective quadrupole phonons or/and phonons of higher multiplicities can improve the agreement. However, it would certainly make the calculations within the PDM-2 more complicate. At least it would increase the number of the parameters of the model unless the structure of phonon operators is defined microscopically in terms of ph pairs as in the RPA. In the meantime a simple way to include effectively the contribution of the missing doorway configurations in the present calculations within the PDM-2 is to add a parameter $\Delta\gamma$ to $\gamma_q^{(\text{PDM2})}(\omega)$ to minimize the discrepancy between $\Gamma_{\text{GDR}}^{(\text{PDM2})}$ and $\Gamma_{\text{GDR}}^{(\text{PDM1})}$. The

strength functions calculated with increasing $\gamma_q^{(\text{PDM2})}(\omega)$ by $\Delta\gamma$ are shown in the right columns (e–h) of Figs. 5 and 6. The overall agreement between theory and experiment is clearly improved. In our opinion it is unlikely that the main features of the results obtained within PDM-1 or PDM-2 (with this additional parameter $\Delta\gamma$) will be altered significantly by more sophisticated microscopic calculations, given the fact that the hot GDR occurs in the stochastization region of high level densities and high excitation energies [28].

This comparison also shows that, despite its simplicity, the PDM-1 has offered a quite reasonable agreement with the data for the width and shape of the hot GDR. The PDM-2, on the other hand, has demonstrated that including explicitly the coupling to higher-order configurations does not change the conclusions of the PDM-1, in particular regarding the weak temperature dependence of the quantal width Γ_Q . This is a clear indication that the quantal effect of complex configurations mixing is relatively insensitive to the change of temperature. Therefore, it can be well incorporated in the parameters of the model selected at $T = 0$ as has been done in PDM-1. The evolution of the GDR shape at $T \neq 0$, therefore, does not depend much on the complexity of the doorway components, but is governed mostly by the presence of the coupling to incoherent pp and hh configurations.

As a prediction of our model we show in Fig. 7 the strength functions of the GDR calculated within PDM-1 at several values of $T > 4$ MeV in ^{120}Sn and $T \geq 2.8$ MeV in ^{208}Pb . The same quantities obtained within PDM-2 are displayed in Fig. 8 using $\Delta\gamma = 0$ (Figs. 8a, b) as well as $\Delta\gamma = 2$ MeV for ^{120}Sn (Fig. 8c) and 0.8 MeV for ^{208}Pb (Fig. 8d). The saturation of the GDR shape is clearly seen at $T \geq 4$ MeV in both nuclei. We hope that these shapes, especially those given in Fig. 7, may serve as references for experimental measurements in future.

3.4. Integrated yield of γ rays

The integrated yields $Y_\gamma^{(i)}$ of γ rays in ^{120}Sn calculated within PDM-1 and PDM-2 are plotted as a function of excitation energy E^* in Fig. 9a, b. The results have been obtained upon performing the integration in Eq. (2.25) within two intervals $12 \text{ MeV} \leq E_\gamma \leq 20 \text{ MeV} + \Delta E_\gamma$ and $12 \text{ MeV} + \Delta E_\gamma \leq E_\gamma \leq 35 \text{ MeV}$. Since the width calculated in PDM-1 is larger than the one obtained within PDM-2, the value of ΔE_γ has been chosen to be 1 MeV (dashed curve) and 2 MeV (dash-dotted curve) within PDM-1, and 0 (solid curve) within PDM-2. These results are compared with the data within 12–20 MeV [9,10] (Fig. 9a) and within 20–35 MeV [10] (Fig. 9b), respectively. The results reproduce reasonably well the observed saturation of the yield in the GDR region. In the region 20–35 MeV (Fig. 9b) the PDM-1 gives somewhat larger values for the integrated yield (dashed and dash-dotted curves) as compared to the data while the results obtained within the PDM-2 (solid curve) are found in a better agreement with the data. In general the trend of saturation of the yield is also reproduced by the PDM in this region. The saturation of the yield at $E^* \geq 300$ MeV is understood here as a natural consequence of the saturation of the GDR shape and its width at $T > 4$ MeV, not by an exceedingly large value of the width as has been proposed previously in Refs. [9,16] -

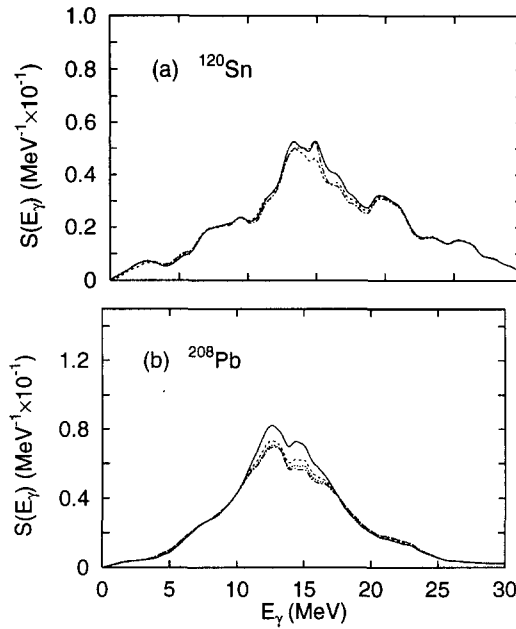


Fig. 7. GDR strength functions calculated within PDM-1 for ^{120}Sn (a) and ^{208}Pb (b) at higher temperatures. In (a): Solid, dashed and dash-dotted curves show the results obtained at $T = 4.1, 5.1$ and 5.8 MeV, respectively. In (b): Solid, dashed, dotted and dash-dotted curves are the results obtained at $T = 2.8, 4, 4.9$ and 6 MeV, respectively. The effect of single-particle has been included in the calculations.

[18]. It is worth noticing that the value of the integrated yield in the region above the GDR (within 20–35 MeV) is more sensitive to the change in the value of ΔE_γ than within the GDR region 12–20 MeV. The reason is that the integration in Eq. (2.25) involved larger energies in the region above the GDR and also that the distribution of the GDR is rather flat in the tail above 20 MeV. As seen in Fig. 9b an increase of ΔE_γ from 2 MeV to 3 MeV reduced noticeably the saturated value of the integrated yield in the region above the GDR. We emphasize that the microscopic structure of the strength function $S_q^{(i)}(\omega)$ with an ω -dependent damping $\gamma_q^{(i)}(\omega)$ is decisively important for an adequate description of both the shape as well as the integrated yield. As shown in Fig. 9c and 9d a Breit–Wigner distribution with a width equal to $\Gamma_{\text{GDR}}^{(i)}$ and centered at ω_{GDR} can describe the integrated yield within the GDR region (Fig. 9c) but strongly overestimates it in the region above 20 MeV (Fig. 9d). Using the FWHM from the Milan model [14] leads to a similar behavior as shown by the dotted curves in Figs. 9c, d. Both the parametrizations for the width proposed in the Catania model [16,17] cannot account for the data of the yields in the GDR region as well as in the region above it as shown by the dash-dotted curves and the curves with crosses. Finally, as a prediction of our model we plot in Fig. 10 the integrated yield of γ rays calculated in the PDM1 and PDM2 within the interval 10–18 MeV and 18–33 MeV for ^{208}Pb . The saturated values of the yield within these intervals amount to around 8×10^{-3} and 1.2×10^{-3} , respectively.

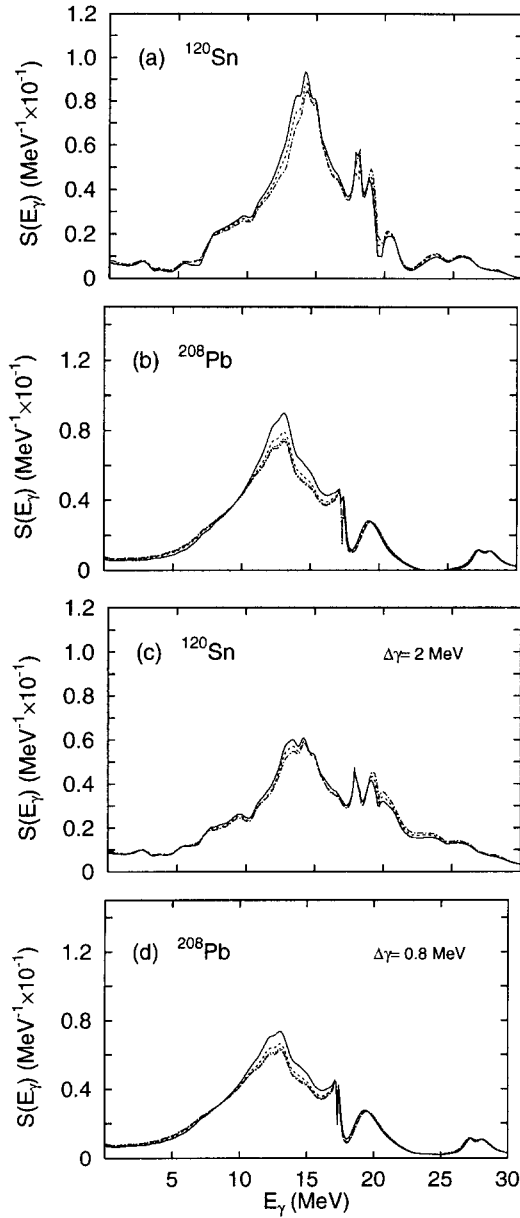


Fig. 8. GDR strength functions calculated within PDM-2 for ^{120}Sn (a,c) and ^{208}Pb (b,d) at higher temperatures. Notations are the same as in Fig. 7. Results in (c) and (d) have been obtained by using $\gamma_q^{(\text{PDM2})}(\omega) + \Delta\gamma$ instead of $\gamma_q^{(\text{PDM2})}(\omega)$.

The present calculations did not include the effects of evaporation width [29] and the GDR equilibration time [30] on the damping of the hot GDR. There is evidence that these effects are small even at high temperatures. Indeed, it has been shown in Ref. [29] that the GDR width should reach a value of around 30 MeV due to the

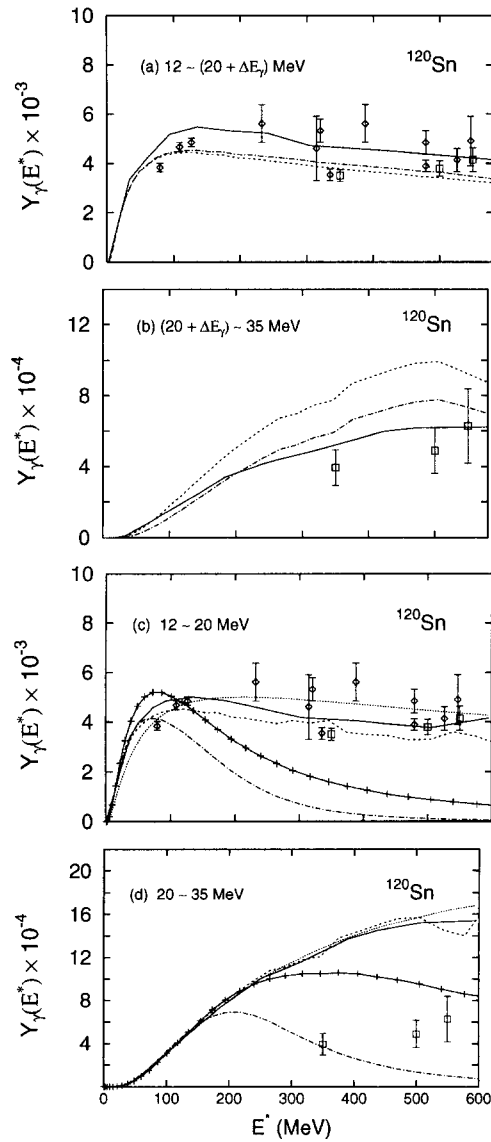


Fig. 9. Integrated yields of the γ rays as a function of excitation energy E^* in ^{120}Sn . Diamonds and squares: data from Refs. [9] and [10], respectively. (a,b): dashed and dash-dotted: the results obtained within PDM-1 with $\Delta E_\gamma = 1$ and 2 MeV, respectively; solid: results obtained within PDM-2 with $\Delta E_\gamma = 0$. (c,d): the results from the calculations using a Breit-Wigner strength function of an ω -independent width Γ_{GDR} centered at ω_{GDR} from different models are shown. Here: dashed and solid: results obtained within PDM-1 and PDM-2, respectively; dotted: results using the width from the Milan model of Ref. [14]; dash-dotted and solid with crosses: results using the parametrizations of the Catania model in Refs. [16] and [17], respectively.

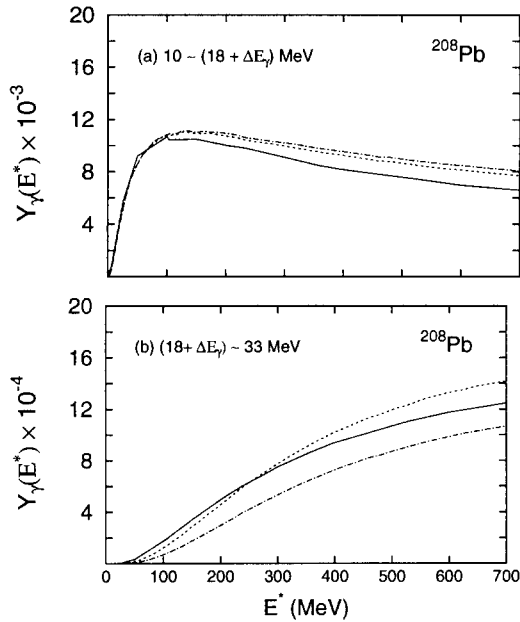


Fig. 10. Integrated yield of the γ rays as a function of excitation energy E^* in ^{208}Pb in the GDR region (a) and in the region above it (b). Notations are the same as in Figs. 9 (a) and (b).

increase of evaporation width at $E^* = 400$ MeV. However, the same reference has also pointed out that, in order to fit the data, one needs to introduce an explicit suppression of the GDR strength when the compound nucleus reaches an excitation energy around 300 MeV. In such a case, the question of the GDR width may become irrelevant above the excitation energy where its strength vanishes or becomes too small. Existing data so far indicate a saturation, rather than an increase, of the GDR width at $E^* > 250$ MeV in good agreement with the results of our calculations. The authors of Ref. [19] have also calculated the strength function of the hot GDR including the evaporation width. They found that the overall spectra resulting from a complete CASCADE calculations are essentially identical to the ones obtained without the evaporation width even for $E^* > 120$ MeV. The contribution of the evaporation width to the total spectrum has been found to be small relatively to the total spectrum including all decay steps. The authors of Ref. [30] proposed to take into account the equilibration time of the GDR, assuming that no GDR is present at the time of formation of the compound nucleus. However, Ref. [10] has pointed out that such a hypothesis is probably reasonable if the projectile and target have the same N/Z ratio. Meanwhile, in Ref. [10], where the saturation of the integrated yield of γ rays has been reported within and above the GDR regions, the N/Z ratios of the two partners are quite different and a substantial dipole moment is present in the entrance channel. This indicates the presence of GDR already before the equilibration is achieved. In our opinion, the quantitative role of the evaporation width and equilibration time in the damping of the hot GDR requires further detailed theoretical studies. More experimental evidence are also needed to confirm whether the

effects of evaporation width and equilibration time on the GDR are really small at high T .

4. Conclusions

In the present paper two versions PDM-1 and PDM-2 of the Phonon Damping Model (PDM) have been applied to a systematic description of three main characteristics of the hot GDR, namely the GDR width, its shape and the integrated yield of γ rays. The results of calculations have been compared with the most recent experimental systematics assessed for these characteristics in ^{120}Sn and ^{208}Pb in the heavy-ion fusion and inelastic α -scattering reactions. An overall agreement between theory and experiment has been consistently achieved for all three characteristics. Predictions have been made for the future measurements of the GDR shapes at higher temperatures up to $T \sim 6$ MeV in ^{120}Sn and ^{208}Pb , and for the integrated yield of γ rays in ^{208}Pb in both regions of the GDR and above it.

The analysis in the present paper allows us to draw the following conclusions.

(1) The PDM describes consistently the rapid increase of the width at low T and its saturation at $T \geq 4$ MeV taking into account the coupling of the GDR to pp and hh configurations at $T \neq 0$. Both the PDM1 and PDM2 have confirmed that the quantal width Γ_Q of the GDR due to coupling to only ph configurations decreases slightly as T increases. It becomes independent of T only when the contribution of two-phonon processes in the expansion to higher-order propagators is neglected.

(2) The PDM is a simple microscopic model yet able to reproduce reasonably well the measured shape of the GDR including some details of its fine structure.

(3) Based on the simplifying assumption of the statistical model the PDM provides a reasonable account for the experimental integrated yield of γ rays using the microscopically calculated width of the GDR. Our model describes well the saturation of the yield in both regions of the GDR and above it, showing a well defined GDR shape up to $T \sim 6$ MeV. This indicates the existence of the hot GDR even at rather high temperatures, provided that the energy-weighted sum rule value is well conserved. As a matter of fact the hot GDR has been observed in ^{120}Sn at rather high excitation energies with a width of around 12 MeV [4,6,10]. In our opinion, since the observed FWHM of the GDR is an averaged quantity, the continuously increasing width, which was inserted in the CASCADE calculations in Ref. [9], should undergo an appropriate averaging procedure before it can be compared with the observed width.

(4) The present versions of the PDM did not yet include a number of effects discussed in the literature, e.g. coupling to continuum, the temperature dependence of single-particle energies, the evaporation width, the GDR equilibration time, the dependence on angular momentum, etc. There have been several references showing that these effects may not be significant at least up to $T \sim 3$ MeV in nuclei with mass number $A \geq 120$ [7,10,11,13,19,31]. The agreement between the results of PDM and the data discussed in the present paper may also serve as an indirect indication that the total

contribution of these effects may not significantly alter the obtained results up to $T \sim 5\text{--}6$ MeV. Nonetheless more detailed studies are required to clarify the explicit contribution of these effects in the high-temperature region.

Acknowledgements

Numerical calculations were carried out by a 64-bit Alpha AXP work-station running Digital UNIX (OSF/1) at the Computer Center of RIKEN. N.D.D. thanks the financial support of the Japan Society for the Promotion of Science.

References

- [1] K. Snover, *Annu. Rev. Nucl. Part. Sci.* 36 (1986) 545;
J.J. Gaardhøje, *Annu. Rev. Nucl. Part. Sci.* 42 (1992) 483.
- [2] J.J. Gaardhøje et al., *Phys. Rev. Lett.* 53 (1984) 148; 56 (1986) 1783.
- [3] D.R. Chakrabarty et al., *Phys. Rev. C* 36 (1987) 1886.
- [4] A. Bracco et al., *Phys. Rev. Lett.* 74 (1995) 3748.
- [5] M. Matiuzzi et al., *Nucl. Phys. A* 612 (1997) 262.
- [6] D. Pierroutsakou et al., *Nucl. Phys. A* 600 (1996) 131.
- [7] G. Enders et al., *Phys. Rev. Lett.* 69 (1992) 249.
- [8] H.J. Hofmann et al., *Nucl. Phys. A* 571 (1994) 301.
- [9] K. Yoshida et al., *Phys. Lett. B* 245 (1990) 7;
J. Kasagi et al., *Nucl. Phys. A* 538 (1992) 585c;
J. Kasagi and K. Yoshida, *Nucl. Phys. A* 557 (1993) 221c.
- [10] P. Piattelli et al., *Nucl. Phys. A* 599 (1996) 63c;
T. Suomijärvi et al., *Phys. Rev. C* 53 (1996) 2258.
- [11] K. Sugawara-Tanabe and K. Tanabe, *Prog. Theor. Phys.* 76 (1986) 1272.
- [12] E. Ramakrishnan et al., *Phys. Rev. Lett.* 76 (1996) 2025; *Phys. Lett. B* 383 (1996) 252.
- [13] T. Baumann et al., *Nucl. Phys. A* 635 (1998) 428.
- [14] R.A. Broglia, B.F. Bortignon and A. Bracco, *Prog. Part. Nucl. Phys.* 28 (1992) 517.
- [15] W.E. Ormand, P.F. Bortignon and R.A. Broglia, *Phys. Rev. Lett.* 77 (1996) 607;
W.E. Ormand et al., *Nucl. Phys. A* 614 (1997) 217.
- [16] P. Chomaz, M. Di Toro and A. Smerzi, *Nucl. Phys. A* 563 509 (1993).
- [17] A. Bonasera, M. Di Toro, A. Smerzi and D.M. Brink, *Nucl. Phys. A* 569 (1994) 215c.
- [18] V. Baran et al., *Nucl. Phys. A* 599 (1996) 29c.
- [19] G. Gervais, M. Thoennessen and W.E. Ormand, *Phys. Rev. C* 58 (1998) 1377R
- [20] N. Dinh Dang, and A. Arima, *Phys. Rev. Lett.* 80 (1998) 4145, *Nucl. Phys. A* 636 (1998) 427.
- [21] N.N. Bogolyubov and S. Tyablikov, *Sov. Phys. Doklady* 4 (1959) 6.
- [22] D.N. Zubarev, *Non-equilibrium Statistical Thermodynamics* (Plenum, New York, 1974); *Sov. Phys. Uspekhi* 3 (1960) 320.
- [23] P.F. Bortignon et al., *Nucl. Phys. A* 460 (1986) 149.
- [24] N. Dinh Dang, *Nucl. Phys. A* 504 (1989) 143.
- [25] P. Donati et al., *Phys. Lett. B* 383 (1996) 15.
- [26] N. Dinh Dang, K. Tanabe and A. Arima, *in Proc. Topical Conference on Giant Resonance* (Varenna, May 11–16, 1998), to be published in *Nucl. Phys. A*; *in Highlights of Modern Nuclear Structure* (Proc. 6th Int. Spring Seminar on Nuclear Physics, S. Agata sui Due Golfi, May 18–22, 1998) (World Scientific, Singapore).
- [27] J.E. Draper et al., *Phys. Rev. Lett.* 49 (1982) 434.
- [28] V. Zelevinsky et al., *Phys. Rep.* 276 (1996) 85.
- [29] Ph. Chomaz, *Phys. Lett. B* 347 (1995) 1.
- [30] P.F. Bortignon et al., *Phys. Rev. Lett.* 67 (1991) 3360.
- [31] H. Sagawa and G.F. Bertsch, *Phys. Lett. B* 146 (1984) 138.